Electronic Supplementary Material (ESI) for Physical Chemistry Chemical Physics.

Supplementary Information

FTIR study of the surface-ligand exchange reaction with glutathione on biocompatible rod-shaped CdSe/CdS semiconductor nanocrystals

Kunisato Kuroi[a*], Masaki Yamada[a], Ibuki Kawamura[a], Minkyo Jung[b], Chan-Gi Pack[cd], Fumihiko Fujii[a*]

[a]*Faculty of Pharmaceutical Sciences, Kobe Gakuin University, Kobe 650-8586, Japan*

[b]*Neural Circuit Research Group, Korea Brain Research Institute, Daegu 41062, Korea*

[c]*Convergence Medicine Research Center (CREDIT), Asan Institute for Life Sciences, Asan Medical Center, Seoul 05505, Korea*

[d]*Department of Convergence Medicine, University of Ulsan College of Medicine, Seoul 05505, Korea*

S-1. Determination of the absorption coefficient of QRs by FCS

The absorption coefficient of QRs at 473 nm was determined by fluorescent correlation spectroscopy (FCS). In FCS measurements, the average number (N) of fluorescent particles existing in the confocal area of the microscope can be determined. By comparing N of GSH-QRs with that of the known extinction coefficient (ε) of a fluorescent dye (Rhodamine 6G (R6G)), ε of GSH-QRs can be determined from the following relationship;

$$N_{\mathrm{GSH-QRs}} : N_{\mathrm{R6G}} = \frac{A_{\mathrm{GSH-Q}}\ \ (473)}{\varepsilon_{\mathrm{GSH-QRs}}(473)} : \frac{A_{\mathrm{R6G}}(473)}{\varepsilon_{\mathrm{R6G}}(473)}$$

where A is the absorbance at 473 nm of a sample solution. On the basis of the previously reported method,[1] $N_{\mathrm{GSH\text{-}QRs}}$ was carefully determined by excitation power-dependent measurements to exclude the possibility of two-photon excitation or blinking behavior of GSH-QRs. Fig. S1 (a) shows the laser power-dependent autocorrelation curves ($G(\tau)$) of GSH-QRs. These curves were fitted to the theoretical expression containing N, described elsewhere,[2] and N was determined as the function of laser power (Fig. S1(b)). $N_{\mathrm{GSH\text{-}QRs}}$ was determined to be 4.7 by extrapolation to the laser power of zero. In the very same manner, N_{R6G} was determined to be 228 (data not shown). In the above relationship, the absorbances of GSH-QRs and R6G at 473 nm were 0.011 and 0.015, respectively. $\varepsilon_{\mathrm{R6G}}(473)$ was calculated to be 18713 $M^{-1}cm^{-1}$ from the literature value ($\varepsilon_{\mathrm{R6G}}(531)$ = 115337 $M^{-1}cm^{-1}$) and its absorption spectrum profile. Taken together these values, $\varepsilon_{\mathrm{QRs}}(473)$ was determined to be 6.8×10^{5} $M^{-1}cm^{-1}$. Because the UV-Vis spectrum of QRs was almost unchanged upon the reaction with GSH (Fig. 1(c)), we assumed that the above absorption coefficient of GSH-QRs is common with TOPO-capped QRs.

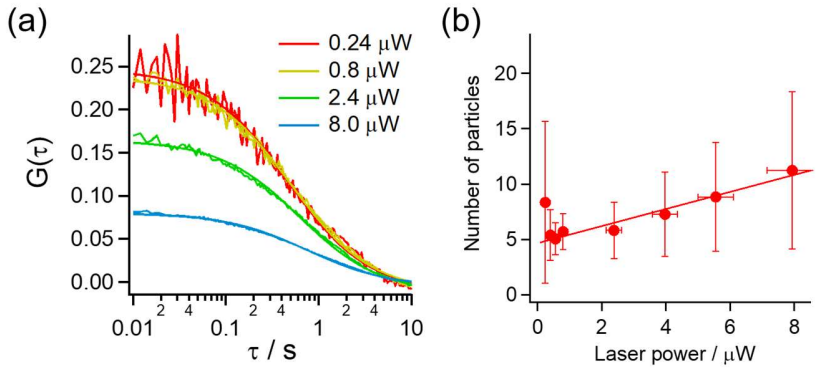

Fig. S1 (a) Excitation laser power dependence of the autocorrelation curve (G(t)) of GSH-QRs. Continuous lines represent fitting curves by the theoretical equation.[2] (b) The average number of GSH-QRs in the confocal volume at various laser powers, determined from fitting of $G(\tau)$ in (a).

Experimental of FCS

FCS measurements were performed on the confocal laser scanning microscopy (Fluoview FV-1000, Olympus) with a 60× objective (NA = 1.2). The output from a 473 nm diode laser was used for excitation. A 20 μL drop of GSH-QRs or Rhodamine 6G in water was put on an 8-well glass chamber and subjected to measurements. Laser power was monitored in front of the objective lens.

REFERENCES

(1) G. Abbandonato, K. Hoffmann, and U. Resch-Genger, Determination of quantum yields of semiconductor nanocrystals at the single emitter level via fluorescence correlation spectroscopy, *Nanoscale*, 2018, **10**, 7147-7154

(2) T. Jin, F. Fujii, Y. Komai, J. Seki, A. Seiyama and Y. Yoshioka, Preparation and Characterization of Highly Fluorescent, Glutathione-coated Near Infrared Quantum Dots for in Vivo Fluorescence Imaging, *Int. J. Mol. Sci.*, 2008, **9**, 2044–2061.

S-2. Quantum yields of QRs and GSH-QRs

The fluorescence quantum yields (QYs) of QRs and GSH-QRs were determined from absorption and fluorescence measurements. The QY of each sample was determined by comparison with the result of rhodamine 6G (R6G) in ethanol as a reference sample under the same measurement conditions. QY was calculated by use of eqn (S1):[1]

$$QY_{\text{sample}} = QY_{\text{R6G}} \frac{m_{\text{sample}}}{m_{\text{R6G}}} \left(\frac{n_{\text{solvent}}}{n_{\text{ethanol}}}\right)^2 \qquad \text{(S1)}$$

where m is a constant relating the absorbance at 480 nm to the integrated fluorescence intensity over the entire spectrum, and n is the refractive index of the solvent. The literature value, QY_{R6G} = 0.94, was used in the calculations.[1]

REFERENCE

(1) Lakowicz, J.R. *Principles of Fluorescence Spectroscopy*, 3rd ed.; Springer, 2006, pp 54-55

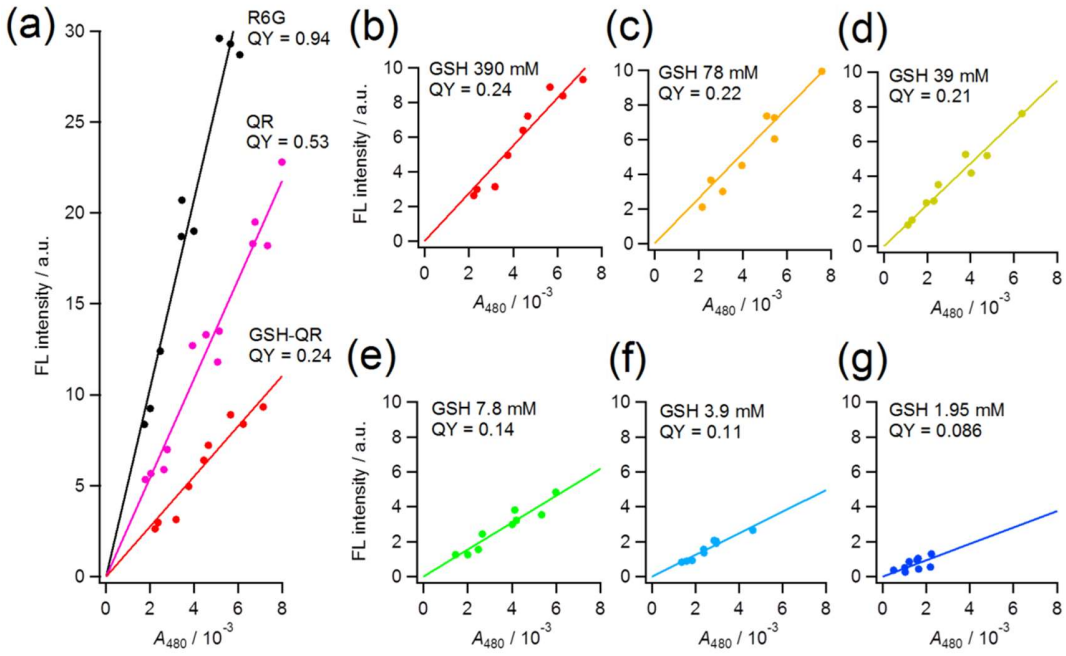

Fig. S2 (a) Plots of the integrated fluorescent intensity versus absorbance at the excitation wavelength (A_{480}) used to determine the quantum yields for R6G, QRs, and GSH-QRs. The linear fits by y = *m*x to obtain *m* in eqn (S1) and determined QY are also shown for each sample. (b)-(g) Similar plots for GSH-QRs at different GSH concentrations.

S-3. IR spectra of TOPO/GSH mixtures

The baseline beneath the TOPO C–H stretching signal at 2920 cm^{-1} was approximated by the following polynomial:

$$f(x) = a\nu^4 + b\nu^3 + c\nu^2 + d\nu + e$$

where ν is the wavenumber, and *a*–*e* are fitting constants. The intensity of the TOPO C–H stretching signal, I_{TOPO}, is defined by

$$I_{TOPO} = A(\nu_{CH}) - f(\nu_{CH}) \qquad (S2)$$

where $A(\nu_{CH})$ is the total absorbance of the IR spectrum at ν_{CH}, and ν_{CH} = ~2920 cm^{-1} is the wavelength of the C–H stretching signal.

The amide region of the IR spectrum (c.a. 1800–1500 cm^{-1}) was decomposed into contributions from the –COOH, amide I, and amide II groups of GSH. Eqn (S3) was used to decompose the spectrum:

$$A(\nu) = a_{COOH}\exp\left(-\left(\frac{\nu - c_{COOH}}{w_{COOH}}\right)^2\right) + a_{\text{amide I}}\exp\left(-\left(\frac{\nu - c_{\text{amide I}}}{w_{\text{amide I}}}\right)^2\right) + a_{\text{amide II}}\exp\left(-\left(\frac{\nu - c_{\text{amide II}}}{w_{\text{amide II}}}\right)^2\right) + \text{offset} \qquad (S3)$$

where $A(\nu)$ is the total absorbance measured at a given wavelength (ν), and *a*, *c*, and *w* represent the intensity, peak location, and bandwidth, respectively, of each Gaussian function. In the fitting by eqn (S3), $w_{\text{amide I}}$ and $w_{\text{amide II}}$ are restricted to be equal. The amide I intensity of GSH (I_{GSH}) is defined as $a_{\text{amide I}}$.

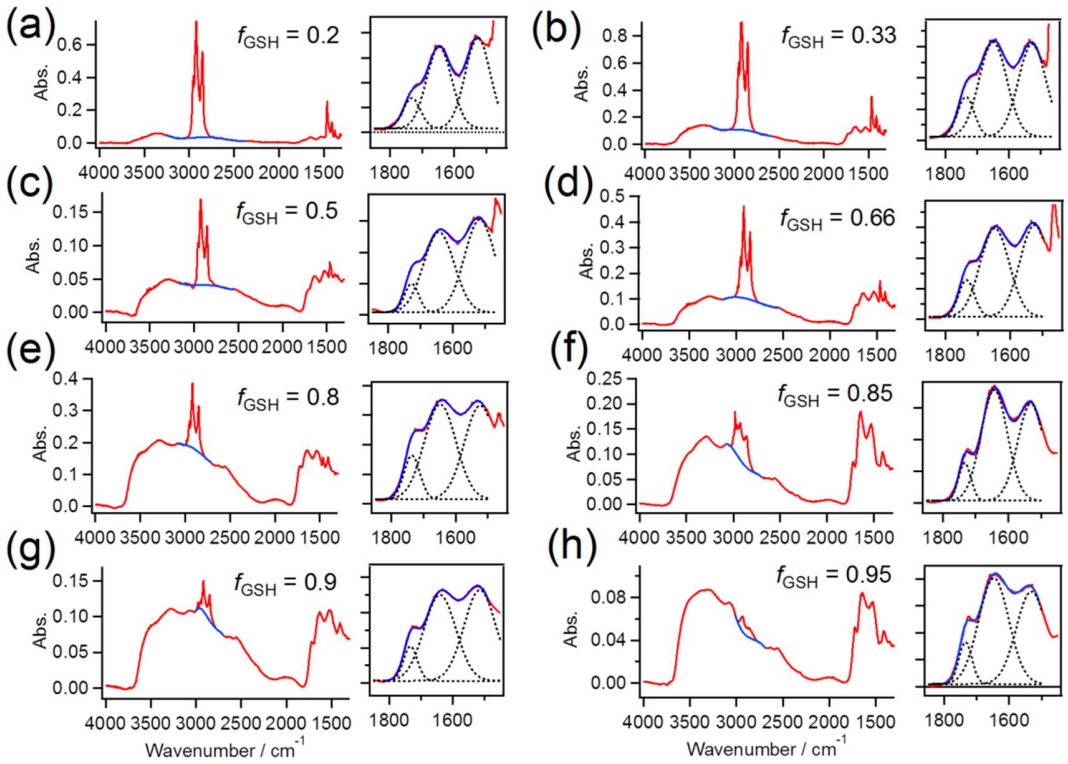

Fig. S3 (a)–(h): IR spectra of TOPO/GSH mixtures at different molar fractions of GSH (f_{GSH}). Expanded spectra at 1450–1850 cm^{-1} are shown at the right of each panel. The baseline beneath the TOPO C–H stretching signal at ~2920 cm^{-1} is approximated by a 4th-order polynomial (see above). Spectral decompositions at 1450–1850 cm^{-1} are represented by Gaussian functions for the three individual components (dotted black lines). The continuous blue line is the sum of the resultant Gaussian fittings.

S-4. Derivation of eqns (1) and (2)

The TOPO (I_{TOPO}) and GSH (I_{GSH}) IR signal intensities are assumed to be proportional to the [TOPO] and [GSH] concentrations in the TOPO/GSH mixtures in the sample films:

$$I_{\mathrm{TOPO}} = k_{\mathrm{TOPO}}[\mathrm{TOPO}], I_{\mathrm{GSH}} = k_{\mathrm{GSH}}[\mathrm{GSH}]$$

where k_{TOPO} and k_{GSH} are the corresponding absorption coefficients. Then, the signal ratio ($X = I_{GSH}/I_{TOPO}$) is expressed as

$$X = \frac{I_{\mathrm{GSH}}}{I_{\mathrm{TOPO}}} = \frac{k_{\mathrm{GSH}}[\mathrm{GSH}]}{k_{\mathrm{TOPO}}[\mathrm{TOPO}]} \equiv M\frac{[\mathrm{GSH}]}{[\mathrm{TOPO}]} \quad \left(M \equiv \frac{k_{\mathrm{GSH}}}{k_{\mathrm{TOPO}}}\right)$$

which rearranges to:

$$\frac{[\mathrm{GSH}]}{[\mathrm{TOPO}]} = \frac{X}{M}$$

The molar fraction of GSH (f_{GSH}) is expressed as,

$$f_{\mathrm{GSH}} = \frac{[\mathrm{GSH}]}{[\mathrm{TOPO}] + [\mathrm{GSH}]} = \frac{\frac{[\mathrm{GSH}]}{[\mathrm{TOPO}]}}{1 + \frac{[\mathrm{GSH}]}{[\mathrm{TOPO}]}} = \frac{X}{M + X}$$

which is presented as eqn (2). Rearrangement of this expression yields eqn (1):

$$X = M\frac{f_{\mathrm{GSH}}}{1 - f_{\mathrm{GSH}}} \quad \left(X = \frac{I_{\mathrm{GSH}}}{I_{\mathrm{TOPO}}},\ M = \frac{k_{\mathrm{GSH}}}{k_{\mathrm{TOPO}}}\right)$$

S-5. IR spectra of GSH-QRs at different concentrations of GSH

The estimated baseline of the TOPO C–H stretching signal is given by an expression same as that in Section S-3. I_{TOPO} is defined by eqn (S2). Spectral decomposition of the amide region was also conducted in the same way, except that a contribution from carboxylate (COO^-) was included. In this case, the total absorbance was expressed as a sum of four Gaussian functions:

$$\begin{aligned} A(\nu) = \; & a_{\mathrm{COOH}} \exp\left(-\left(\frac{\nu - c_{\mathrm{COOH}}}{w_{\mathrm{COOH}}}\right)^2\right) + a_{\mathrm{amide\ I}} \exp\left(-\left(\frac{\nu - c_{\mathrm{amide\ I}}}{w_{\mathrm{amide\ I}}}\right)^2\right) \\ & + a_{\mathrm{COO^-}} \exp\left(-\left(\frac{\nu - c_{\mathrm{COO^-}}}{w_{\mathrm{COO^-}}}\right)^2\right) + a_{\mathrm{amide\ II}} \exp\left(-\left(\frac{\nu - c_{\mathrm{amide\ II}}}{w_{\mathrm{amide\ II}}}\right)^2\right) \\ & + \mathrm{offset} \end{aligned} \tag{S4}$$

In the fitting by eqn (S4), $w_{\mathrm{amide\ I}}$, $w_{\mathrm{COO^-}}$, and $w_{\mathrm{amide\ II}}$ were fixed to be equal. The amide I intensity of GSH (I_{GSH}) is defined as $a_{\mathrm{amide\ I}}$.

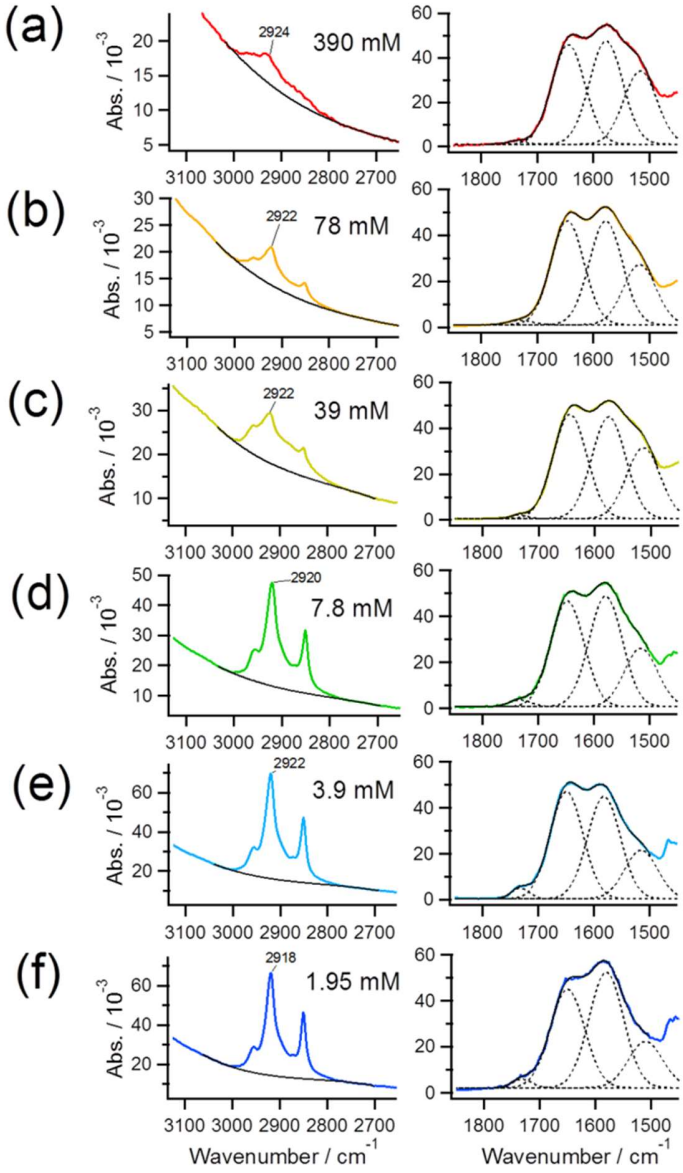

Fig. S4 IR spectra of GSH-QRs at GSH concentrations of 390 (a), 78 (b), 39 (c), 7.8 (d), 3.9 (e), and 1.95 mM (f). Spectra in the C–H stretching and amide regions are shown on the left and right, respectively. The baselines for TOPO C–H stretching signal and spectral decompositions in the amide region are shown by black continuous lines and dotted lines, respectively.

S-6. GSH concentration dependence of the IR signal ratio (I_{GSH} / I_{TOPO})

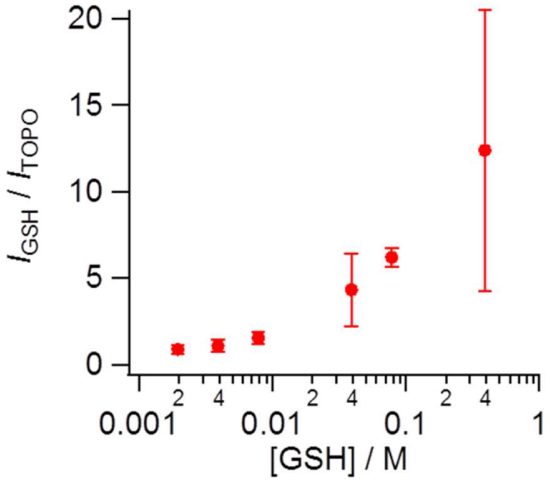

Fig. S5 Plot of the GSH to TOPO signal ratio (I_{GSH}/I_{TOPO}) versus the concentration of GSH. Plot was constructed from the IR spectra in Fig. 4(a) and Fig. S4.